

# Accepted Manuscript

Full length article

Comparing the microstructure and mechanical properties of *Bombyx mori* and *Antheraea pernyi* cocoon composites

Juan Guan, Wenshu Zhu, Binghe Liu, Kang Yang, Fritz Vollrath, Jun Xu

PII: S1742-7061(16)30515-3

DOI: <http://dx.doi.org/10.1016/j.actbio.2016.09.042>

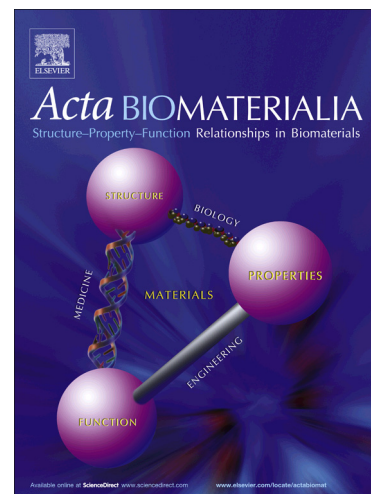
Reference: ACTBIO 4463

To appear in: *Acta Biomaterialia*

Received Date: 6 June 2016

Revised Date: 7 September 2016

Accepted Date: 28 September 2016



Please cite this article as: Guan, J., Zhu, W., Liu, B., Yang, K., Vollrath, F., Xu, J., Comparing the microstructure and mechanical properties of *Bombyx mori* and *Antheraea pernyi* cocoon composites, *Acta Biomaterialia* (2016), doi: <http://dx.doi.org/10.1016/j.actbio.2016.09.042>

This is a PDF file of an unedited manuscript that has been accepted for publication. As a service to our customers we are providing this early version of the manuscript. The manuscript will undergo copyediting, typesetting, and review of the resulting proof before it is published in its final form. Please note that during the production process errors may be discovered which could affect the content, and all legal disclaimers that apply to the journal pertain.

# Comparing the microstructure and mechanical properties of *Bombyx mori* and *Antheraea pernyi* cocoon composites

Juan Guan<sup>\*1,2</sup>, Wenshu Zhu<sup>1</sup>, Binghe Liu<sup>3</sup>, Kang Yang<sup>1</sup>, Fritz Vollrath<sup>4</sup>, Jun Xu<sup>\*3,5</sup>

<sup>1</sup> School of Materials Science and Engineering and Intl. Research Center for Advanced Structural and

Biomaterials, Beihang University, Beijing, China, 100191

<sup>2</sup> State Key Laboratory of Molecular Engineering of Polymers, Fudan University, Shanghai, China, 200433

<sup>3</sup> Department of Automotive Engineering, School of Transportation Science and Engineering and Advanced

Vehicle Research Center (AVRC), Beihang University, Beijing, China, 100191

<sup>4</sup> Department of Zoology, University of Oxford, Oxford, UK, OX1 3PS

<sup>5</sup> State Key Laboratory of Automotive Safety and Energy, Tsinghua University, Beijing, China, 100084

\* Corresponding authors:

Juan Guan, [juan.guan@buaa.edu.cn](mailto:juan.guan@buaa.edu.cn); Telephone 0086 15810741731; Postal address: IRC 418, Beihang University, No. 37 Xue Yuan Road, Hai Dian District, Beijing, 100191, China

Jun Xu, [junxu@buaa.edu.cn](mailto:junxu@buaa.edu.cn); Telephone 0086 1082339923; Postal address: Rm 1801, Bai Yan Building, Beihang University, No. 37 Xue Yuan Road, Hai Dian District, Beijing, 100191, China

**Abstract:**

Silkworm cocoon material is a natural composite consisting of silk fibres and sericin glues. Domestic and wild silkworms both produce cocoons but with different functionality- one selected by man for textile manufacture whereas the other selected by Nature to provide damage-tolerant housing. To understand the structure-property relationship of cocoons, we evaluated and compared the microstructure and mechanical properties of two representative cocoon walls. It appears that a “brittle and weak” composite is produced by domestic *Bombyx mori* (*B. mori*) while a “tough and strong” composite is made by wild *Antheraea pernyi* (*A. pernyi*). The superior mechanical performance of *A. pernyi* cocoons can be attributed to both the material properties and the fibre network microstructures. Failure mechanisms and different failure modes for cocoon fibre composites were also proposed. A finite element model revealed qualitatively the effect of fibre properties and inter-fibre bonding strength on the mechanical properties of the fibre network. It emerged that both good mechanical properties of fibres and robust inter-fibre bonding, were required for tough and strong fibre composites. The new insights could inspire new designs of synthetic fibre composites with enhanced mechanical properties.

**Keywords:** fibre composite; non-woven; microstructure; mechanical properties; stress transfer

## 1. Introduction

Protein-based silk cocoon composites constructed by silkworms are an attractive group of light and tough natural composites [1-4], inspiring research as well as commercialisation [5-7]. *Bombyx mori* (*B. mori*) silkworm has been cultivated in-house by humans for thousands of years to produce valuable textile fibres. The wild, in the other hand, harbors a huge diversity of different species of silkworms, of which the best known is perhaps *Anthearea pernyi* (*A. pernyi*). As protective housing, wild cocoons have excellent mechanical properties such as high modulus, wear and impact resistance [8-11]. It appears that wild cocoons have evolved for protection against diverse threats as well as to regulate the internal environment by controlling the flow of water or gases such as oxygen and carbon dioxide [12, 13]. Still *A. pernyi* cocoons can also be unwound and woven into luxury fabrics [14-16], although the calcium oxalate crystal in *A. pernyi* cocoon makes such utilization difficult [17-19]. The cocoons produced by the two species can represent two distinct types of natural fibre composites as *B. mori* has been bred by humans for the collection of its silk fibre while *A. pernyi* faces very different selection pressures in the wild.

Recently, Chen *et al.* have published a series of articles on the morphology and physical properties of 27 different species of silkworm cocoons [8, 20]. Cocoon morphology can be described very broadly as non-woven fibre composite similar to electro-spun fibre mat. However, each class of cocoons demonstrates diversity in detailed structural features such as open or closed structure, degree of non-woven structure, numbers of layers and extra components such as calcium oxalates. Moreover, cocoon walls as natural polymer "macro-balloons" share many similarities with man-made polymeric microspheres such as low apparent density, great specific surface area and comparable compressive strength [9, 21]. Morphologically, *B. mori* cocoon consists of outer floss,

cocoon shell, pupa and ecdysis; whereas *A. pernyi* cocoon possesses extra cocoon grip or peduncle and minerals [8, 18, 20]. Concerning physical properties, *B. mori* cocoons can be categorized as ‘weak’ cocoons with high porosity while *A. pernyi* cocoons would be ‘tough’ cocoons with medium porosity. Exploration of the detailed property and structural differences between cocoon classes might provide inspirations for the design synthetic fibre composites.

On the mechanical properties and failure mechanisms of fibre composites, a number of models were proposed and widely used. Carlsson *et al* outlined a shear-lag approach to predict the tensile strength of paper composite [22]. Essentially, the fibre length and relative bonded area are the two important factors determining the fracture behaviour of the paper composite; and fibre pull-out is expected to decrease with higher relative bonded area or stronger fibre/fibre bonds. Other investigators built a fibre network model using mean-field approximation [23]. In this model, the stress could be transferred among the segments of long fibres at the fibre-fibre crossings. The model also sets length distribution instead of uniform length between crossings to explain non-specific fibre networks. Notably, Chen *et al.* proposed a cocoon connectivity model based on the different structural contributions of the component and the porosity [24]. It was observed that during the mechanical test, the modulus of a cocoon shell sample decreased with increasing stress and strain, and may or may not go through a ‘yield’ zone, which sets apart tough and brittle cocoons. Chen *et al* suggested that the damage through loss of bonding connectivity between fibres gradually reduces the stiffness of the composite with increasing strain. More importantly, this model showed that modulus is a function of the network density and the fibre dimensions, which relates the macroscopic modulus of the composite to the microstructure. However, it was found that the tensile mechanical properties of cocoon composite were not in positive correlation with the fibre

properties. Consequently, it is not fully understood how tough cocoons have evolved microstructures that are able to realize the observed superior mechanical properties.

Here we demonstrate how both materials properties or silk fibre's properties and cocoon's microstructural parameters affect the final mechanical properties of the cocoon composite. We also discuss the failure behaviours of the cocoon composites, and under what condition the failure behaviour of cocoons could be revised. From this we extract critical parameters in the design of natural fibre composites, which could improve our knowledge in making better synthetic fibre composites.

## 2. Materials and methods

### 2.1. Materials

*B. mori* cocoons were purchased from Shanghai Buke Medical Co. Ltd. and the source region of these cocoons was Zhejiang Province, China. *A. pernyi* cocoons were purchased from a professional silk rearing farmer in Liaoning Province, China. All the cocoons were stored under the same environmental conditions in the laboratory (temperature of 25 °C and low humidity <50% to prevent the live pupas from hatching). Being invertebrates, both silkworm species are currently not protected by any legislations from experimental use and all silkworm pupae removed from cocoons were disposed as biological waste.

The cocoon wall specimens were prepared by carefully cutting open the cocoon along its long axis and removing the pupas inside. For tensile testing of cocoon walls, dog-bone shaped specimens were cut along the long axis of the cocoon ellipsoid; and the middle section of the *B. mori* dog-bone specimens were cut with different widths (1, 2, 3, 5 mm) and 10 mm length; for *A. pernyi*

specimens the length was 15 mm.

The fibres were unravelled carefully from the cocoon walls with minimal stretching especially for highly cross-linked *A. pernyi* cocoon. About 5 mm long fibre was mounted onto a designed paper frame to facilitate the sample loading.

## 2.2. Quasi-static tensile and compressive tests on cocoon walls

Quasi-static tensile tests on cocoon wall samples were performed at room temperature using the materials testing system (MTS, model e44) with a 200N load cell (precision grade of 0.5%). More than 10 dog-bone cocoon specimens were tested for each width under the same environmental conditions at a nominal strain rate  $1.00 \times 10^{-1} \text{ s}^{-1}$  for *B. mori* and  $6.67 \times 10^{-2}$  for *A. pernyi* (which fall within the quasi-static loading domain). All results are reported as mean  $\pm$  standard deviation. The thicknesses of the samples were measured using a micrometre with a consistent compressive stress. All the dog-bone specimens were marked and placed in plastic bags before and after the experiment. Stress was derived from the measured raw force data whereas the strain was derived from the crossbeam displacement. The initial modulus of cocoon composite was calculated as the slope of the stress-strain curve below 10MPa stress with linear fit  $R^2 > 0.9$ . This method was also used for silk fibre modulus calculations with the stress threshold of 50MPa.

Compressive mechanical tests on cocoon walls were performed on a DMA Q800 (TA Instruments, Waters Ltd.) under controlled force mode as strain rate mode causes control problems of the instrument. Compressive tests were carried out up to a high stress level of 1.0 MPa for circular cocoon samples (diameter of 4.7 mm) at room temperature. Force ramp rate was 0.5 N/min.

### 2.3. Compositional analysis

Compositional analysis was performed by weighing the cocoon samples before and after degumming for both cocoons as well as also after demineralization for *A. pernyi* cocoons. For degumming, a common procedure with  $\text{Na}_2\text{CO}_3$  was used [25]. Dry cocoon samples were immersed in  $\text{Na}_2\text{CO}_3$  solution (0.5 wt.%, 100 mL) for 1 hr at 80°C under stirring, and then rinsed with running tap water for 3 hrs before washing with deionized water and finally dried for 24hrs at 35°C. For demineralization, the Gheysens procedure [19] was followed. *A. pernyi* cocoon walls were immersed in EDTA or edetic acid disodium salt solution (1mol/L, 600mL, pH adjusted to 10 with NaOH) and gently stirred to remove mineral calcium oxalate for 72hrs at 40°C. The cocoon taken out of EDTA solution was rinsed with running tap water for 10hrs, washed with deionized water and dried in an oven with full ventilation for 24 hrs at 35°C. The weight loss after degumming and demineralization was recorded using a lab balance with an accuracy of 0.1mg. Five tests were repeated for both *B. mori* and *A. pernyi* cocoons.

### 2.4. Tensile tests on cocoon fibres

Tensile mechanical tests on cocoon fibres were performed on a DMA Q800 (TA Instruments, Waters Ltd.) under strain-rate mode. The strain rate was  $3.33 \times 10^{-3} \text{ s}^{-1}$ . About 15 fibre samples carefully taken from the outer layer of the cocoon wall were tested for each cocoon type. The gauge length was 5mm.

### 2.5. Scanning electron microscopy and image analysis

Cocoon wall samples were fixed onto the platform using conductive tape and sputter-coated



with palladium for 120s. Bundled silk fibres were put through a thin tube and cut into short sections for the cross-sectional view of the fibres before applying the same sputter-coating procedure. Scanning electron microscope (SEM) images of cocoon walls and fibre sections were taken on a JSM 6010 at 20kV accelerating voltage.

The morphological parameters were measured or derived from the SEM images using image processing software ImageJ. The intersectional fibre length  $l$  was measured as the distance of the fibre between two adjacent intersections on the inner-most cocoon layers, and the final  $l$  was presented as the average of >20 measurements. The fibre width  $d$  was also measured on the inner-most layer and an average value was presented. About 30 cross-sections of the fibre for each cocoon were chosen from the cross-sectional images and measured, and an average cross-sectional area was calculated and presented. This procedure of measuring cross-sectional area was established elsewhere [26].

## 2.6. Statistical analysis

Morphological data and mechanical properties in Table 1 and Fig. 1B, C, E, F were presented as the mean values and standard deviation or  $M \pm SD$  from multiple measurements. The number of measurements was introduced in each relevant section. In analysing the significant differences between two samples of the same property (for example, the maximum stress and corresponding strain, initial modulus and breaking energy), two-sample t-test was used to determine the statistical significance. Statistical significance was designated with \* $p < 0.05$ , \*\* $p < 0.01$  and \*\*\* $p < 0.001$ .

## 2.7. Finite Element Analysis

To further demonstrate different failure mechanisms which is difficult to show by experiment,

finite element analysis was conducted. The FEA model contains both geometrical structural information and non-linearity of material properties along with complicated boundary conditions which cannot be simply solved by explicit analysis. The commercial software ABAQUS was employed for modelling the representative volume element (RVE) model of the cocoon composite. The long and short beam elements were used to represent the fibre and the sericin component where they mainly subjected to tension rather than compression, respectively. The classical beam element B31 type in ABAQUS was chosen for this study. According to the convergence analysis, 0.002 mm mesh size of fibre and 0.001 mm mesh size of sericin are chosen with total number of 1632 elements.

Without the loss of generality, the RVE model was modelled with eight fibroin fibres, arranged in mesh with crossing angles of  $60^\circ$  (as measured from the microstructural images of the cocoon inside surface). Every two fibres at the intersection were connected by a beam element representing sericin, and the sericin and the fibre were connected through “coupling” constraint where the displacements of the connectors are exactly the same in related nodes; four ends of the fibres on one side were fixed, and on the other side another four ends of fibres were applied load. This artificial design results in a load-bearing fibre-network connected by the beam elements of sericin and all the fibroin fibres could share load simultaneously. There are three major failure mode of a fibre reinforced composite materials, e.g. fibre failure, matrix (sericin) failure and coupling failure. Current FEA model may not accurately enough to represent the coupling failure mode but it should be representative enough to describe the first two failure modes.

To compare and reveal the two failure modes for *B. mori* and *A. pernyi*, we constructed two sets of cocoon models. The first set compared *B. mori* and *A. pernyi* cocoons using respectively a weak or strong network, and fibre properties based on the experimental results. An intermediate model

was introduced to create a weak *B. mori* network with stronger and tougher *A. pernyi* silks. In the second set, the same strong fibre network was used for five cocoon models, and the fibre properties were derived from reference [8] for different species of silks. The network strength difference was achieved in the FE model by introducing different sizes to the sericin beam including the diameter and the length. For weak inter-fibre bonding networks (*B. mori* model I and Intermediate model), the diameter and the length of the sericin beam were 7  $\mu\text{m}$  and 4  $\mu\text{m}$ ; and for strong networks (*A. pernyi*. I, II and others) 20  $\mu\text{m}$  and 0.5  $\mu\text{m}$  were used. The fibre property parameters from our experiments and reference [8] were extracted and presented in Table 2 (section 4.5). The five cocoon models based on reference [8] are *A. pernyi*, *Bombyx mandarina* (*B. mandarina*), *Bombyx mori* (*B. mori*), *Gonometa postica* (*G. postica*) and *Opodiphthera eucalypti* (*O. eucalypti*).

The Elastic-linear strengthen model [27] was selected to present the mechanical properties of the fibroin fibre and the sericin glue, written as:

$$\begin{aligned} \varepsilon &= \frac{\sigma}{E}, & \text{when } \sigma < \sigma_0 \\ \varepsilon &= \frac{\sigma_0}{E} + \frac{1}{E_t}(\sigma - \sigma_0), & \text{when } \sigma \geq \sigma_0 \end{aligned}$$

where  $\varepsilon$  is the strain;  $\sigma$  is the stress;  $\sigma_0$  is the yield stress;  $E$  is the Young's modulus and  $E_t$  is the tangent modulus. The parameters  $\sigma_0$ ,  $E$ , and  $E_t$  of the fibre and sericin glue were fitted from the stress-strain curves from our measurements, reference [8] and [24]. The failure criterion is chosen as strain failure criterion for both the fibre and the sericin, which is also used for the spider silk in the previous study [28]. The element will be deleted when the strain reaches the failure strain in simulation process to trigger the failure. The results of the sericin were  $E_{glue}=28.5$  MPa,  $E_0$ ,  $glue=28.5$  MPa,  $E_{t,glue}=2.625$  MPa and failure strain 0.12; and the results for fibres were presented later in section 4.5.

### 3. Results

#### 3.1. Tensile mechanical properties of cocoon composites

The tensile stress-strain curves and the tensile mechanical properties of *B. mori* and *A. pernyi* cocoon walls of different sample widths are shown in Fig. 1(A, D). The maximum stress and corresponding strain, initial modulus at stress <10 MPa and breaking energy as a toughness measure (calculated from the accumulated stress-strain area prior to the maximum stress) is defined as  $\sigma_m$ ,  $\epsilon_m$ ,  $M_i$  and  $E_b$  respectively, and plotted in Fig. 1(B, C, E, F). For the 2 mm sample width, *B. mori* failed at  $\sigma_m=25$  MPa and  $\epsilon_m=0.16$  without yielding; whereas *A. pernyi* failed at much higher  $\sigma_m=55$  MPa and  $\epsilon_m=0.25$ . It is apparent that for almost all the widths studied *A. pernyi* cocoons were 2 times stronger and 5 times tougher. Moreover, *A. pernyi* cocoons were able to transit to a post-yield stage with an obvious yield at 0.05-0.1 strain until failure, which suggests a toughened behaviour.

The tensile stress-strain behaviours of both *B. mori* and *A. pernyi* cocoons showed a sample-width dependence. For *B. mori*, both  $\epsilon_m$  and  $E_b$  clearly increased with increasing sample width; and  $\sigma_m$  increased significantly from 19 MPa for 1 mm to 25 MPa for 3 mm, whereas  $M_i$  showed an opposite decreasing trend from 3.0 MPa for 2 mm to 1.7 MPa for 5 mm. For *A. pernyi*, the changes in  $\sigma_m$  and  $M_i$  were not as significant with increasing width from 1 mm to 3 mm. In addition, the sharpest increase in  $\epsilon_m$  and  $E_b$  of *A. pernyi* occurred between width 1 mm and 2 mm, and  $\epsilon_m$  maintained 0.25 and  $E_b$  maintained 12 MJ m<sup>-3</sup> for width 2-5 mm.

#### 3.2. Composition analysis and sericin distribution

As shown in Fig. 2(A), *B. mori* cocoon contained about 71.8% silk fibroin and 28.2% sericin, whereas *A. pernyi* cocoon contained a substantial 84.3% of silk fibroin, about 8.7% sericin and 7.0%

mineral. Our measured value in the *A. pernyi* cocoon wall matches well with a reported sericin content of less than 8% of the total weight of the raw silk [29]. Fig. 2(B) clearly shows that, morphologically, the sericin-spread on the *B. mori* fibre was a few micrometres thick. However, *A. pernyi*'s sericin layer could not be distinguished from the fibre's cross-section, indeed it is reported to be only 200~300 nm thick [30]. Although the minerals are critical for the hardness and impact resistance of wild cocoons [18], here we did not consider their contributions to the tensile mechanical behaviour of cocoon walls, given that these crystals are small and disconnected in the outer-most layer as shown in the inset of Fig. 4(B).

### 3.3. Tensile mechanical properties of cocoon silk fibres

Raw silk fibres were carefully unravelled from both *B. mori* and *A. pernyi* cocoons and tested under quasi-static tensile mode, Fig. 3 shows the stress-strain curves of these fibres. Both silk fibres displayed features of three-stage tensile behaviour: the initial, high-modulus region was followed by the yield and the post-yield low-modulus region. Shaded areas show the range and variability of stress-strain behaviours of these fibres. The marked blue curves denote representative curves for extraction of the FE property parameters. The results of fibre property parameters of the marked curves are listed in Table 2, together with other fibre properties. *A. pernyi* silk fibres displayed a larger variability in stress-strain behaviours, which was explained previously [31], but  $\epsilon_m$  for *A. pernyi* was significantly higher than for *B. mori*. Moreover, *A. pernyi* fibres had greater initial and tangent moduli.

### 3.4. Microstructure, density and porosity of cocoon walls

The SEM images of morphology and microstructure of *B. mori* and *A. pernyi* cocoons are

shown in Fig. 4; and the microstructural parameters along with other physical property parameters such as porosity are summarised in Table 1. Both cocoon types showed a non-woven composite structure with twin silk fibres coated with sericin and preferential orientation of the fibres was not observed. In the image analysis, two geometric parameters, the intersectional fibre length  $l$  and the fibre width  $d$  were introduced.  $l$  was measured as the centre-to-centre distance between two neighbouring fibre intersections; and  $d$  was measured as the diameter of the fibre. A geometry parameter  $k$  to take both  $l$  and  $d$  into account was calculated as  $d^2/l$ , which will be discussed in section 4.3. *A. pernyi* cocoons possessed longer intersectional fibre length (187  $\mu\text{m}$ ) but larger fibre width ( $\sim 54 \mu\text{m}$ ). More notably, *A. pernyi* cocoons had a lower degree of areal porosity than *B. mori*, in agreement with Zhang *et al.* [10]. The difference in porosity can also be seen in the cross sections of cocoon walls: *B. mori* contained loose and multiple layers with apparent inter-layer gaps while as *A. pernyi* had only one dense and compact layer. Concerning the morphology of single fibres, *B. mori* fibres mostly possessed round or irregular cross-sections, whereas *A. pernyi* fibres were flat ribbon-shaped.

The apparent density of the cocoon walls was determined by conducting compressive mechanical tests perpendicular to cocoon walls. As shown in Fig. 5, with increasing compressive stress the density also increased for both cocoons at first very fast. At low stress of 0.1 MPa, the density is 250  $\text{kg}\cdot\text{m}^{-3}$  for *B. mori* and 450  $\text{kg}\cdot\text{m}^{-3}$  for *A. pernyi*, comparable to those reported by Chen [20] and Zhang [32]. Although *A. pernyi* had a greater density, the specific strength of 0.11 MPa/[ $\text{kg}\cdot\text{m}^{-3}$ ] for *A. pernyi* was still greater than 0.08 MPa/[ $\text{kg}\cdot\text{m}^{-3}$ ] for *B. mori*, and the specific toughness of *A. pernyi* cocoon was 3 times that of *B. mori*.

**Table 1** Comparison of microstructural and physical property parameters between *A. pernyi* and *B.*

*mori* cocoons.

Types of cocoon	<i>B. mori</i>	<i>A. pernyi</i>
Intersectional fibre length $l$	$120 \pm 24 \mu\text{m}$	$187 \pm 80 \mu\text{m}$
Fibre sectional shape	Triangular; irregular	Flat ribbon
Fibre width $d$	$18 \pm 2 \mu\text{m}$	$54 \pm 5 \mu\text{m}$
Density	$250 \text{ kg} \cdot \text{m}^{-3}$	$450 \text{ kg} \cdot \text{m}^{-3}$
Sericin layer thickness	$2 \mu\text{m}$	$0.2\text{-}0.3 \mu\text{m}$
Cocoon porosity	75%	58%
Geometric parameter $k$	2.7	15.3

As the porosity ( $n$ ) cannot be easily measured, we derived it from the apparent density ( $\rho_a$ ) and the fibre density ( $\rho_f$ ) of cocoon walls using the following relationship:

$$n = 1 - \frac{\rho_a}{\rho_f}$$

Taking  $\rho_f$  to be  $1300 \text{ kg m}^{-3}$  for solid fibres and the above measured density for cocoons, *A. pernyi*'s porosity turned out to be 58% compared to 75% for *B. mori*. The lower porosity of *A. pernyi* is consistent with the microstructural observations shown in Fig. 4, which could further infer a much stronger fibre network.

#### 4. Discussion

Different sample widths for cocoon samples were examined in the tensile tests to show the effect of continuous fibre length, because the whole cocoon composite contains only one continuous fibre and the cocoon microstructure is complex. By decreasing the sample width, we reduced the continuous fibre length and also effectively reduced the number of inter-fibre bonds or bonding strength. The width dependence of cocoon properties suggests that the stress transfer along continuous silk fibres may play an important role in the cocoon mechanical properties, which

suggests that fibre composites with greater continuous fibre length should differ from short-fibre composites such as paper.

#### 4.1 The effect of sample width on the tensile properties of cocoons

Statistical analysis showed there was a “softening” effect (or significant decrease in  $M_i$ ) when increasing sample width from 2mm to 5mm on *B. mori* and from 3mm to 5mm for *A. pernyi*. According to the “connectivity” model proposed by Chen *et al.* [20], the modulus of the cocoon composite is contributed by the moduli of the fibroin fibre ( $M_1$ ), sericin ( $M_2$ ) and the inter-fibre bonding ( $M_3$ ), and  $M_1 > M_2 > M_3$ . In samples of wider-widths the composite modulus may have been skewed lower due to the higher contribution from the inter-fibre bonding modulus  $M_3$ . Interestingly, there was also a “strengthening” effect (or significant increase in  $\sigma_m$ ) when increasing sample width from 1mm to 2mm for both *B. mori* and *A. pernyi*, which may be explained by Carlsson’s theory [22]. With increased sample width and continuous fibre length, stress transfer and load share might be enhanced. Thus more fibres could be involved to enhance the composite’s strength  $\sigma_m$ . We might be able to deduce the effective distance for stress transfer through continuous fibre from this experiment, which showed that the effective distance for stress transfer in *B. mori* was around 2mm, beyond which width  $\sigma_m$  no longer increased. This distance was about 17 times of the intersectional fibre length of 120 $\mu$ m as observed in the microstructural section. Similarly, the distance for effective stress transfer in *A. pernyi* was about 2 mm (about 11 times of the intersectional fibre length of 187  $\mu$ m).

#### 4.2 Materials properties of the fibre and sericin: intrinsic contributions

We confirmed that *A. pernyi* cocoon possessed a significantly lower sericin fraction, which in



itself is surprising in the context of the function of this tough composite. This observation agrees with the previous report [33]. Although the sericin content varies depending on the layers as the outer layer often possesses much higher sericin content, the sericin content on average for the two cocoons is significantly different. If *A. pernyi* represents a “stronger” fibre network, it may be expected to utilize a greater content of fibre-binder. Nevertheless, the sericin as an amorphous and hydrophilic protein with much smaller molecular weight, was shown to possess much lower strength and modulus (130 MPa and 3.5 GPa) than the fibroin fibre [24]. Therefore, incorporating less sericin in the cocoon composite may be a strategy for *A. pernyi* cocoons to achieve better mechanical properties.

Although there is a great variability in the tensile mechanical properties for fibres from each cocoon, as previously reported [26, 29, 31, 34, 35], the toughness of *A. pernyi* fibres is generally greater than that of *B. mori*. Zhang *et al.* reported the tensile properties of four kinds of degummed single silk fibres. For example, the strength for *B. mori* fibres ( $635 \pm 108$  MPa) is higher than *A. pernyi* ( $426 \pm 55$  MPa), however, benefited from the larger strain, the breaking energy value (toughness) of *A. pernyi* fibre is  $130 \text{ MJ} \cdot \text{m}^{-3}$  and the value of *B. mori* fibre is  $100 \text{ MJ} \cdot \text{m}^{-3}$  [32, 36]. Other publications showed a toughness range  $123\text{-}175 \text{ MJ} \cdot \text{m}^{-3}$  of reeled *A. pernyi* fibre [29], and  $78\text{-}107 \text{ MJ} \cdot \text{m}^{-3}$  of reeled *B. mori* fibre [36, 37]. When the fibres were reeled without degumming, the values of the strength and breaking energy were lower [29]. This toughness difference in silk fibres should suggest that the tougher mechanical performance of *A. pernyi* cocoon composites may come from the higher-toughness *A. pernyi* fibres. On the other hand, although *B. mori* silk fibres are less tough than *A. pernyi* fibres, they remain a high-performance biopolymer fibre. However, the cocoon composite displayed weak and brittle performance which mismatches the fibre properties.

This leads us to argue that good properties of the constituent fibres are only the intrinsic reason for the cocoon composite properties, and are not sufficient for strong and tough composite as will be discussed next.

In addition, the different molecular structures in both silk fibroin and sericin including the primary structure of the amino acid sequence are clearly ascribed for the property differences of the fibres, as discussed in a recent publication [38]. The possible effect of the different primary structures of the fibre fibroin on cocoon's mechanical properties can be reflected via the mechanical properties of the fibres, which will be discussed in the finite element modelling section.

#### 4.3 Microstructures of the fibre network: extrinsic contributions

Based on the microstructural results, the main microstructural differences in the two cocoons are illustrated in Fig. 4(G) and (H): *B. mori* has thin fibres and shorter intersectional fibre distance; whereas *A. pernyi* has thick fibres and longer intersectional distance. Although the intersectional fibre length for *A. pernyi* was greater, the fibre width was also greater. The former would decrease the bonding density / network strength, whereas the latter would increase the bonding density / network strength. In order to reflect the combined effect, we defined a geometric parameter  $k$  (as the square of fibre width  $d^2$  divided by the intersectional fibre length  $l$ ), which can indicate the network strength in cocoons. As shown in Table 1, *A. pernyi*'s  $k$  is five times greater than *B. mori*'s, which indicates a much stronger network strength. We note that the flat and ribbon type of morphology of *A. pernyi* fibres was shown previously to have an impact on the mechanical properties [29]. This suggests that wider *A. pernyi* fibres can provide greater inter-sectional bonding area than the triangular *B. mori* fibres. Moreover, the flat morphology of *A. pernyi* fibre

could be more densely packed into cocoons, thus contributing to the higher density and lower porosity.

Besides, the sericin layer was much thinner for in *A. pernyi* filaments, which might result in a stronger inter-fibre bonding due to increased shear stiffness in the binder layer. The effect caused by decreasing the sericin layer thickness from a few micrometres to several hundred nanometres can be easily demonstrated in the finite element analysis later. In addition, thinner sericin layers, would make for easier stress transfers. We propose that this thinner bonding layer gives *A. pernyi* another advantage in the microstructure for stronger bonding and more effective stress transfer.

#### 4.4 Tensile failure modes for cocoon composites

Fig. 6(A-D) compares the failure morphology of the two cocoons. Failed *B. mori* cocoon wall samples, showed broken sericin bonding and unravelled fibre network while broken and fibrillated fibres were seen in *A. pernyi* samples while the network structure remained stable not far from the fracture path. This suggests two very different failure modes for the fibre composites: *B. mori* failed as a destabilized network and *A. pernyi* failed as fractured fibres.

Stress transfer theory allows us to explain these differences in failure behaviour. As shown earlier, *B. mori* cocoons did not have sufficient inter-fibre bonding in the microstructure to transfer stress, thus the weaker binder sericin would first fail where the stress is concentrated to cause disconnections of fibres, which then induces catastrophic failure of the network. In contrast, *A. pernyi* cocoon presented a more effective fibre network structure with stronger inter-fibre bonding through denser fibre packing, greater bonding area and much thinner layer of sericin bonding. With more effective stress transfer and load share via stronger inter-fibre bonding, *A. pernyi* could

coordinate the stress state of individual fibres, maintain the network structure and eventually exploit fibres' full strength. Comparing the two failure behaviours, we deduce that in the much weaker fibre network of *B. mori* destabilization of the fibre network occurs before the fibres' strength could be exerted; and the strong network of *A. pernyi* ensured that the fibres could share load to provide a strong and tough composite performance. Overall, this suggests that for a strong and tough fibre composite a robust fibre network is the prerequisite, within which stress could be effectively shared and the fibre properties could then play the part.

#### 4.5 Finite Element Modelling (FEM)

The analysis of the material behaviour leads us to hypothesize that fibre properties as well as fibre network properties contribute to the strength and toughness of *B. mori* and *A. pernyi* cocoons. Although the importance of a robust fibre network was clearly demonstrated by comparing *B. mori* and *A. pernyi*, it is not clear whether strong and tough fibres are also a requirement for strong and tough cocoon performance. In this section we put forward two sets of comparisons separately considering the extrinsic and intrinsic contributions:

- (1) *B. mori* model I: weak network with measured *B. mori* fibre properties; intermediate model: weak network with measured *A. pernyi* fibre properties; and *A. pernyi* model I: strong network with measured *A. pernyi* fibre properties;
- (2) A series of strong network cocoon models with varying fibre properties: *B. mori* model II; *A. pernyi* model II; *B. mandarina* model; *G. postica* model and *O. eucalypti* model.

**Table 2** Fibre property parameters referred to in the FEM methods and simulations.

Types of silk	Young's modulus (MPa)	Yield stress (MPa)	Tangent modulus (MPa)	Failure strain
---------------	--------------------------	-----------------------	--------------------------	-------------------

This work	<i>A. pernyi</i>	9633	245	1959	0.247
	<i>B. mori</i>	7456	319	1112	0.149
Ref. [8]	<i>A. pernyi</i>	6231	142	1404	0.29
	<i>B. mandarina</i>	7491	221.5	1344	0.26
	<i>B. mori</i>	8232	313	1264	0.13
	<i>G. postica</i>	6620	83.36	1131	0.24
	<i>O. eucalypti</i>	7460	130	2652	0.0475

In construction of finite element models (FEMs), as shown in Fig. 7(A), we created a fibre network and fixed short beams of sericin at each inter-fibre crossings, which could be changed in the cross-sectional area and the length to simulate varied inter-fibre bonding strengths. For strong network cocoon models, shorter length and larger cross-sectional area were assigned to the sericin beams, corresponding to thinner sericin layer and greater intersectional bonding area. For weak networks, the longer length and smaller cross-sectional area were assigned. The simulated tensile curves of *B. mori* model I, intermediate model and *A. pernyi* model I are shown in Fig. 7(B). The blue curve of *B. mori* cocoon model I displayed a much lower breaking load compared to the black curve of *A. pernyi* cocoon model, which showed four times larger breaking load. The red curve of the intermediate model with improved fibre properties from *B. mori* to *A. pernyi* almost overlaid on top of *B. mori* model I, which did not seem to change the brittleness of the cocoon composite. This implies that, without a strong network, strong fibre properties alone would not improve cocoon performance. Moreover, from the stress diagrams in Fig. 6(E) in line with the SEM images, we observed similar features for cocoon failures- destabilised network structure with broken sericin beam for *B. mori* cocoon model I and fractured fibres for *A. pernyi* cocoon model I. Notably, the fracture path for *A. pernyi* cocoon follows a deflected jig-jag way, which agrees with the microstructural observation and further proves *A. pernyi* cocoon is able to resist tensile fracture and

provides a toughened behaviour. These models clearly reveal the differences in failure modes of the two subject cocoon composites.

In another comparison of varied fibre properties (as listed in Table 2), a series of strong network cocoon models were constructed with the tensile curves shown in Fig. 7(C). After introducing a strong network to *B. mori* cocoon model II, the simulated max. force could be increased nearly four times. This suggests that, with essentially the same *B. mori* fibres, the maximum tensile load of the cocoon composite could be increased to a much greater level simply by enhancing the fibre network. *O. eucalypti* cocoon model displayed the weakest and most brittle behaviour, although its fibres were not weak but brittle compared to other fibres. This model stands in contrast to the *A. pernyi* cocoon model II, whose fibres had much greater failure strain. Owing to the brittleness of the fibre, *O. eucalypti* model's strong network could not help since the fibres were easily broken. In other words, the composite with brittle fibres showed fibre fractures at much lower load, which validates the hypothesis that without good fibres even a strongly bonded network cannot produce a strong and tough composite. Besides, the *B. mandarina* and *G. postica* cocoon models with enhanced fibre network both belonged to tough cocoons similar to *A. pernyi*, although *B. mandarina* was the strongest and *A. pernyi* had the greatest failure strain. Nevertheless, these three tough cocoons showed varied mechanical behaviours under the complex interplay of the fibre property parameters, e.g. modulus and failure strain. To summarise the section of FEM, we have shown that both strong fibre network and good fibres (such as in *A. pernyi*) contribute to the tensile mechanical properties and failure behaviours of a tough and strong fibre composite.

## 5. Conclusions

*B. mori* and *A. pernyi* cocoon composites share a similar fibre-network structure with fibroin fibres overlapped and connected by sericin binder. Tensile mechanical tests showed that *B. mori* cocoon behaved as a weak and brittle fibre composite while as *A. pernyi* behaved strong and tough. SEM imagery also revealed that *B. mori* failed as a destabilised fibre network with broken sericin; whereas *A. pernyi* failed with fractured fibres across the fracture path and the rest of the fibre network remained stable. Despite this, *A. pernyi* had a higher density and lower porosity with a specific breaking energy 3 times greater than that of *B. mori*. The tensile properties of the two cocoon fibres were both tough although *A. pernyi* displayed greater failure strain and toughness. Moreover, the microstructures of the two cocoons were different in several ways. One of the microstructural features of *A. pernyi* cocoon was its flat fibre shape which provided greater bonding area; another feature was that *A. pernyi* possessed a significantly lower fraction of sericin binder, which spread only a few hundred nanometres thick onto the fibres. These microstructural features combine to provide *A. pernyi* cocoon a much stronger fibre network.

We were able to translate both the materials properties and the microstructural information into different settings in establishing finite element models for understanding the mechanical behaviours of cocoon composites. For *A. pernyi* cocoon, the connection sericin beams used shorter length and greater cross-sectional area to result in a strong fibre network with enhanced inter-fibre bonding. The distinct failure modes for *B. mori* and *A. pernyi* were visualised and confirmed the experimental measurements. Importantly, we showed that a tough and strong fibre composite could be made through re-design of the microstructure and effectively introducing stronger inter-fibre bonding. The new insights can guide the design of novel fibre composites or non-wovens with desirable and

predictable mechanical properties.

## 6. Acknowledgements

GJ thanks the support from the National Natural Science Foundation of China [51503009], the State Key Laboratory of Molecular Engineering of Polymer (Fudan University) [K2016-05], and Beihang University. FV thanks AFOSR grant FA9550-15-1-0264. JX thanks the support from start-up funds of “The Recruitment Program of Global Experts” awardee from Beihang University [YWF-16-RSC-011] and Opening fund of State Key Laboratory of Automotive Safety and Energy, Tsinghua University [KF16142].

## 7. References

- [1] [Chen F, Porter D, Vollrath F. Silk cocoon \(\*Bombyx mori\*\): Multi-layer structure and mechanical properties. \*Acta Biomaterialia\* 2012;8:2620-7.](#)
- [2] [Kundu SC, Dash BC, Dash R, Kaplan DL. Natural protective glue protein, sericin bioengineered by silkworms: Potential for biomedical and biotechnological applications. \*Progress in Polymer Science\* 2008;33:998-1012.](#)
- [3] [Zhao H, Feng X, Yu S, Cui W, Zou F. Mechanical properties of silkworm cocoons. \*Polymer\* 2005;46:10.](#)
- [4] [Chen X, Chandra N. The effect of heterogeneity on plane wave propagation through layered composites. \*Composites Science and Technology\* 2004;64:1477-93.](#)
- [5] [Zhang K, Si FW, Duan HL, Wang J. Microstructures and mechanical properties of silks of silkworm and honeybee. \*Acta Biomaterialia\* 2010;6:2165-71.](#)
- [6] [Melke J, Midha S, Ghosh S, Ito K, Hofmann S. Silk fibroin as biomaterial for bone tissue engineering. \*Acta Biomaterialia\* 2016;31:1-16.](#)
- [7] [Rockwood D, Preda R, Yucel T, Wang X, Lovett M, Kaplan D. Materials fabrication from \*Bombyx mori\* silk fibroin. \*Nature Protocols\* 2011;6:1612-31.](#)
- [8] [Chen F, Porter D, Vollrath F. Structure and physical properties of silkworm cocoons. \*Journal of the Royal Society Interface\* 2012;9:2299-308.](#)
- [9] [Shah D, Vollrath F, Porter D. Silk cocoons as natural macro-balloon fillers in novel](#)



polyurethane-based syntactic foams. *Polymer* 2015;56:9.

[10] Zhang J, Kaur J, Rajkhowa R, Li JL, Liu XY, Wang XG. Mechanical properties and structure of silkworm cocoons: A comparative study of *Bombyx mori*, *Antheraea assamensis*, *Antheraea pernyi* and *Antheraea mylitta* silkworm cocoons. *Materials Science & Engineering C-Materials for Biological Applications* 2013;33:3206-13.

[11] Xu J, Zhang W, Gao X, Meng W, Guan J. Strain Rate and Anisotropic Microstructure Dependent Mechanical Behaviors of Silkworm Cocoon Shells. *PloS one* 2016. p. e0149931.

[12] Blossman-Myer B, Burggren W. The silk cocoon of the silkworm, *Bombyx mori*: Macro structure and its influence on transmural diffusion of oxygen and water vapor. *Comparative Biochemistry and Physiology Part A: Molecular & Integrative Physiology* 2010;155:259-63.

[13] Gauthier N, Mandon N, Renault S, Bénédet F. The *Acrolepiopsis assectella* silk cocoon: Kairomonal function and chemical characterisation. *Journal of Insect Physiology* 2004;50:1065-74.

[14] Liu X, Xing T, Xu D, Chen G. Study on novel eco-friendly anti-creasing agents for natural silk fabric. *Chinese Chemical Letters* 2012;23:665-8.

[15] Tsukada M, Arai T, Winkler S. Chemical modification of tussah silk with acid anhydrides. *Journal of Applied Polymer Science* 2000;78:382-91.

[16] Eadie L, Ghosh TK. Biomimicry in textiles: past, present and potential. An overview. *Journal of The Royal Society Interface* 2011;8:761-75.

[17] Kako TKA. Whiteness, hardness and dyeing properties of tussah *Antheraea pernyi* silk fabrics treated with chitosan after one-bath degumming and bleaching. *Journal of Sericultural Science of Japan (Japan)* 1998;67.

[18] Kaur J, Rajkhowa R, Tsuzuki T, Wang X. Crystals in *Antheraea assamensis* silkworm cocoon: Their removal, recovery and roles. *Materials & Design* 2015;88:236-44.

[19] Gheysens T, Collins A, Raina S, Vollrath F, Knight DP. Demineralization Enables Reeling of Wild Silkmoth Cocoons. *Biomacromolecules* 2011;12:2257-66.

[20] Chen F, Porter D, Vollrath F. Morphology and structure of silkworm cocoons. *Materials Science and Engineering: C* 2012;32:772-8.

[21] Huang SQ, Zhao HP, Feng XQ, Cui W, Lin Z, Xu MQ. Mechanical properties of cocoons constructed consecutively by a single silkworm caterpillar, *Bombyx mori*. *Acta Mechanica Sinica* 2008;24:151-60.

[22] Carlsson L, Lindstrom T. A shear-lag approach to the tensile strength of paper. *Composites Science and Technology* 2005;65:183-9.

[23] Astrom J, Makinen J, Alava M, Timonen J. Elasticity of Poissonian fiber networks. *Physical Review E, Statistical Physics, Plasmas, Fluids, And Related Interdisciplinary Topics* 2000;61.

[24] Chen F, Porter D, Vollrath F. Silkworm cocoons inspire models for random fiber and particulate composites. *Physical Review E* 2010;82:6.

[25] Cao T, Wang Y, Zhang Y. Effect of Strongly Alkaline Electrolyzed Water on Silk Degumming and the Physical Properties of the Fibroin Fiber. *Plos One* 2013;8:8.

- [26] [Guan J, Porter D, Vollrath F. Silks cope with stress by tuning their mechanical properties under load. \*Polymer\* 2012;53:2717-26.](#)
- [27] [Bertram A. Elasticity and Plasticity of Large Deformations. \*Spectrochimica Acta Part A: Molecular and Biomolecular Spectroscopy\* 2005;Springer Berlin:21.](#)
- [28] [Cranford SW, Tarakanova A, Pugno NM, Buehler MJ. Nonlinear material behaviour of spider silk yields robust webs. \*Nature\* 2012;482:72-U91.](#)
- [29] [Fu CDXFZ. Understanding the Mechanical Properties of Antheraea Pernyi Silk-From Primary Structure to Condensed Structure of the Protein. \*Advanced Functional Materials\* 2011;21:9.](#)
- [30] [Fu C, Porter D, Shao Z. Moisture Effects on Antheraea pernyi Silk's Mechanical Property. \*MACROMOLECULES\* 2009;42:4.](#)
- [31] [Wang Y, Guan J, Hawkins N, Porter D, Shao Z. Understanding the variability of properties in Antheraea pernyi silk fibres. \*Soft matter\* 2014;10:6321-31.](#)
- [32] [Zhang J, Rajkhowa R, Li JL, Liu XY, Wang XG. Silkworm cocoon as natural material and structure for thermal insulation. \*Materials & Design\* 2013;49:842-9.](#)
- [33] [Kaur J, Rajkhowa R, Tsuzuki T, Millington K, Zhang J, Wang XG. Photoprotection by Silk Cocoons. \*Biomacromolecules\* 2013;14:3660-7.](#)
- [34] [Rajkhowa R, Kaur J, Wang XG, Batchelor W. Intrinsic tensile properties of cocoon silk fibres can be estimated by removing flaws through repeated tensile tests. \*Journal of the Royal Society Interface\* 2015;12:10.](#)
- [35] [Zhang J, Du S, Kafi A, Fox B, Li JL, Liu XY, et al. Surface energy of silk fibroin and mechanical properties of silk cocoon composites. \*Rsc Advances\* 2015;5:1640-7.](#)
- [36] [Porter D, Guan J, Vollrath F. Spider silk: super material or thin fibre? \*Adv Mater\* 2013;25:1275-9.](#)
- [37] [Shao Z, Vollrath F. Surprising strength of silkworm silk. \*Nature\* 2002;418:741.](#)
- [38] [Malay AD, Sato R, Yazawa K, Watanabe H, Ifuku N, Masunaga H, et al. Relationships between physical properties and sequence in silkworm silks. \*Scientific Reports\* 2016;6:11.](#)

Figure Captions:

Fig. 1 Tensile behaviour of *B. mori* (A)-(C) and *A. pernyi* (D)-(F) cocoon specimens with different parallel widths. (A) and (D) present the stress-strain curves; and (B), (C), (E) and (F) are the derived properties including max. stress  $\sigma_m$ , strain at max. stress  $\varepsilon_m$ , initial modulus  $M_i$ , and area under the curve as breaking energy  $E_b$ .

Fig. 2 Composition analysis of *B. mori* and *A. pernyi* (A) and images of sericin enwrapped microstructural morphology of *B. mori* in cross section(B) and *A. pernyi* inside surface(C). Scale bars represent 20  $\mu\text{m}$ .

Fig. 3 Stress-strain curves of raw silk fibres from *B. mori* (A) and *A. pernyi* (B) cocoons.

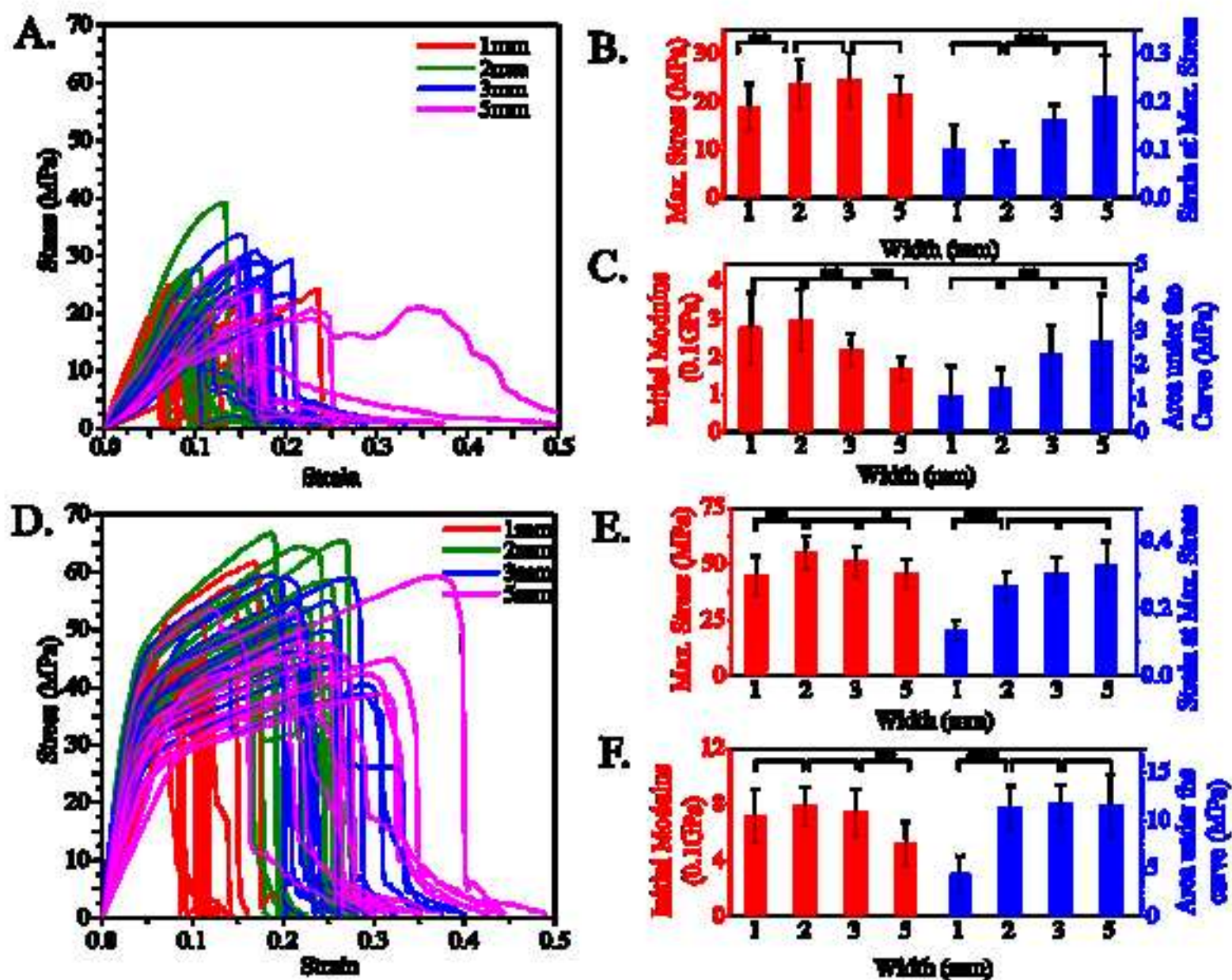
Fig. 4 SEM images of morphology and microstructure of *B. mori* (left panel) and *A. pernyi* (right panel) cocoons. (A) and (B) are microstructures of the cocoon outside surface; (C) and (D) are microstructures of the cocoon inside surface; (E) and (F) are the microstructures of the cocoon shell cross-section and (G) and (H) are abstract structure of the natural cocoon shell. All scale bars (except the insert in (B)) represent 100  $\mu\text{m}$ .

Fig. 5 Compressive behaviour of cocoon walls, shown as density as a function of compressive stress for *B. mori* (A) and *A. pernyi* (B) cocoon wall. The green lines and numbers indicate the median density at 0 and 1.0 MPa compressive stress; and the black lines indicate the compressive stress.

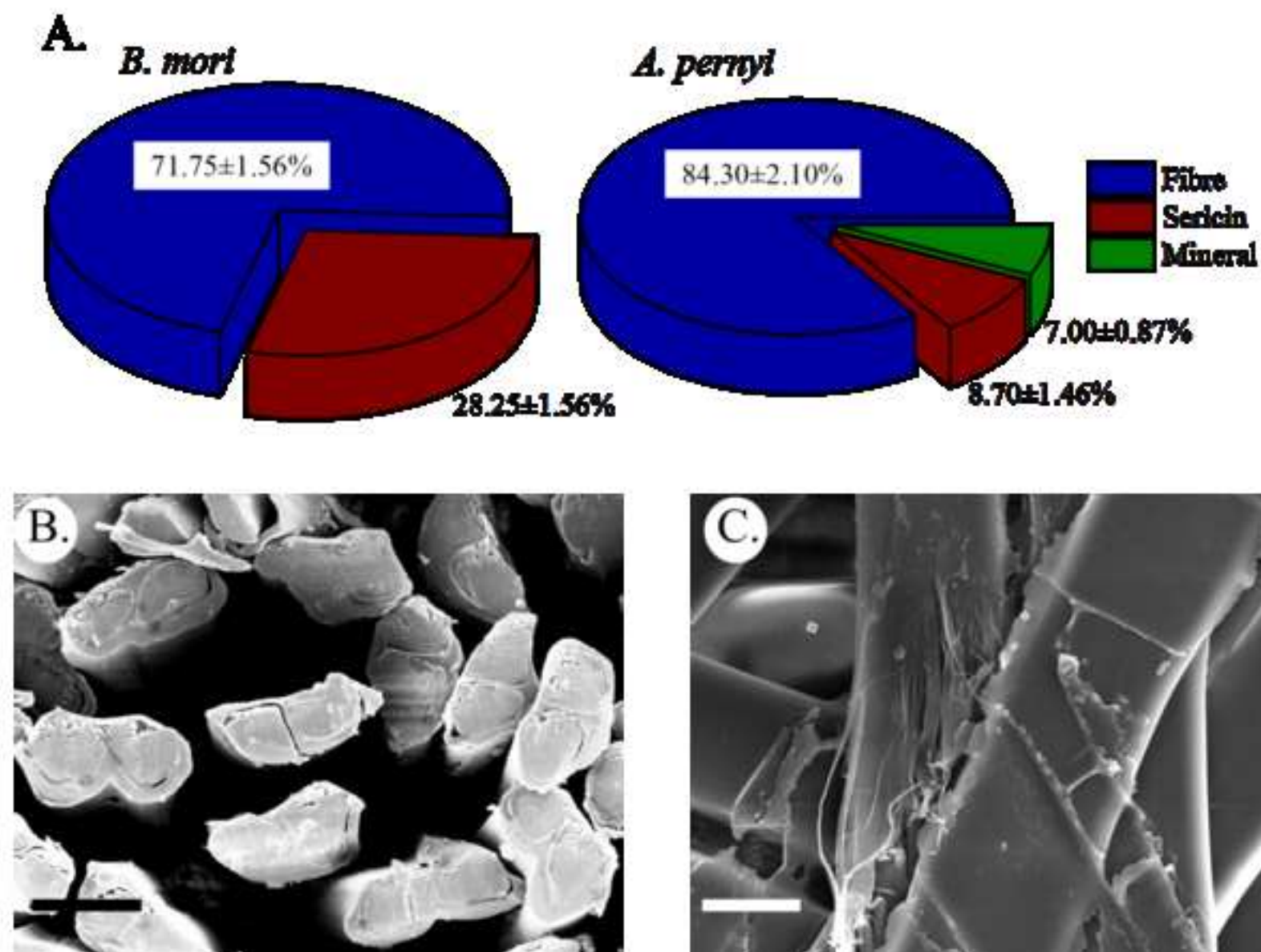
Fig. 6 Microstructural images of the cocoon samples after tensile failure of *B. mori* (A), (C) and *A.*

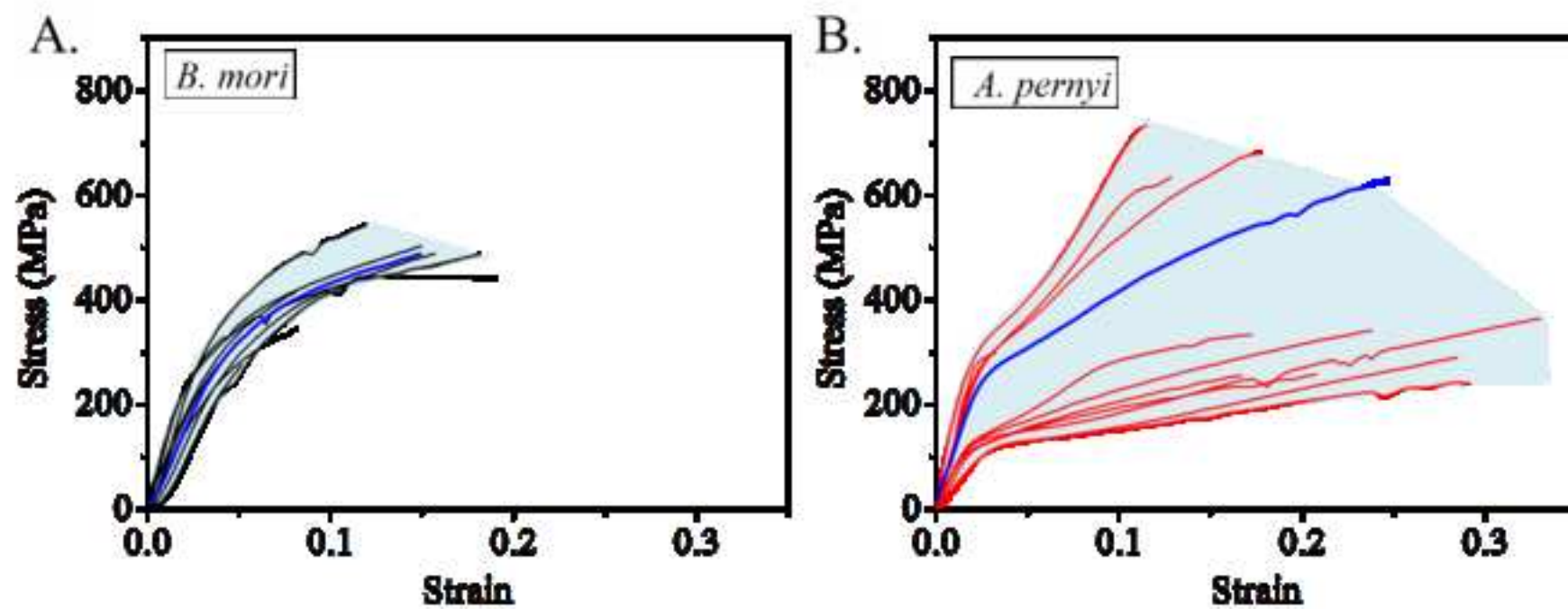
*pernyi* (B), (D) and the Von Mises stress  $\sigma_{Mises}$  evolution in the structure and the different failure types of *B. mori* and *A. pernyi* cocoons (E). Scale bars represent in (A) and (B) are 500  $\mu\text{m}$  and 50  $\mu\text{m}$  in (C) and (D), respectively.

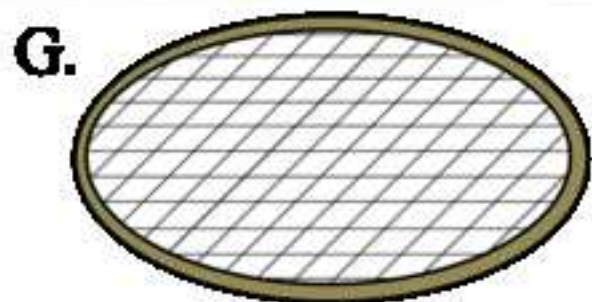
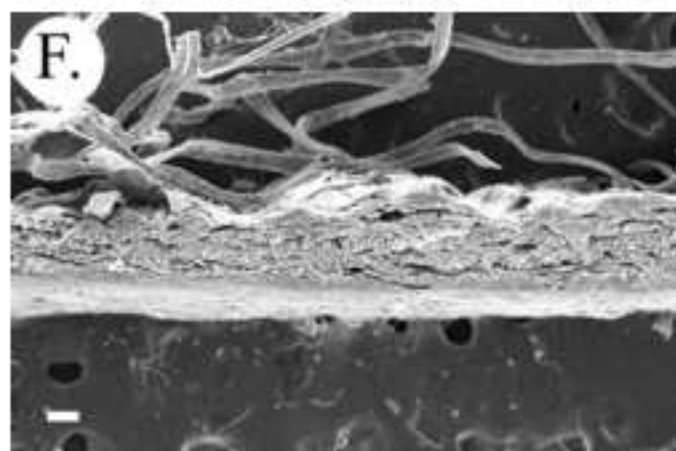
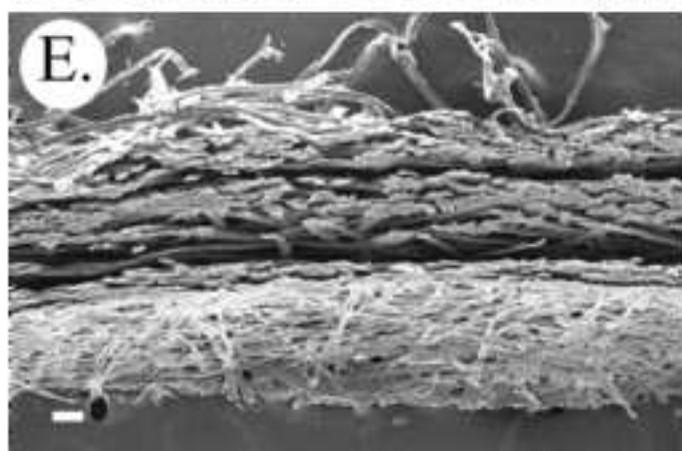
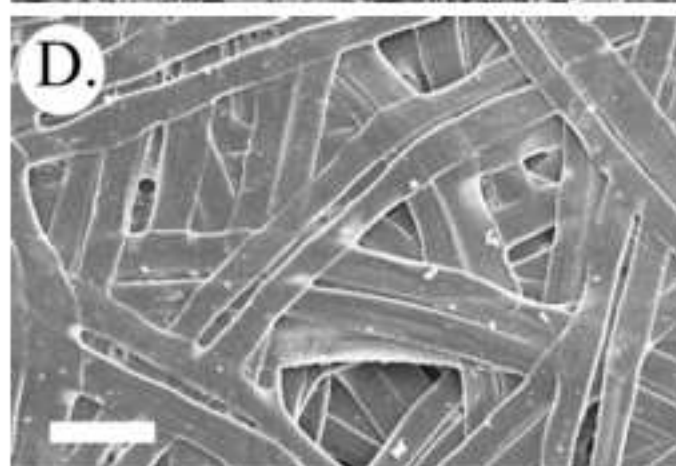
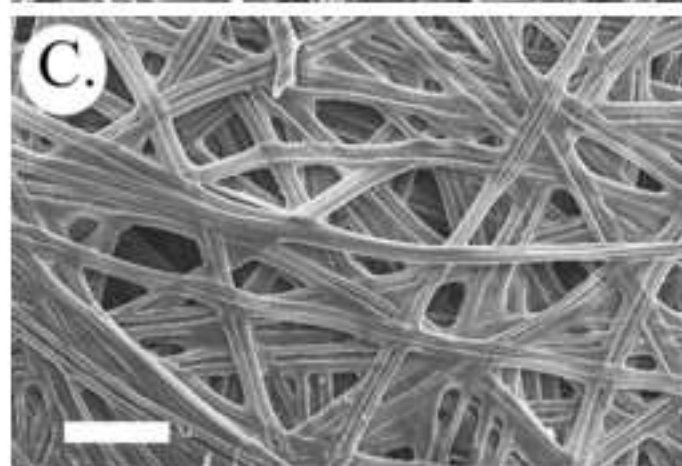
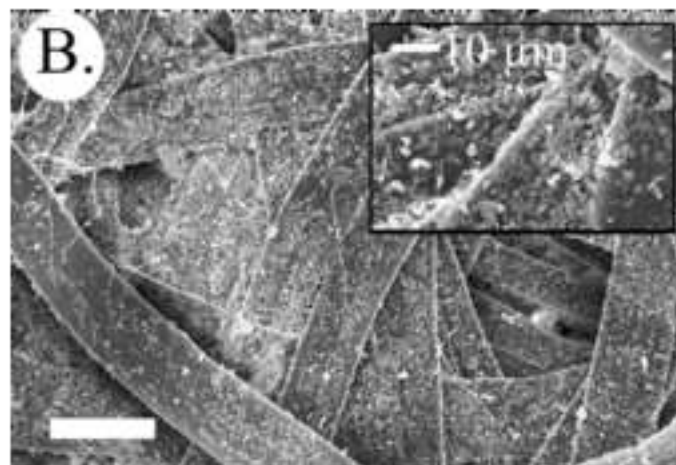
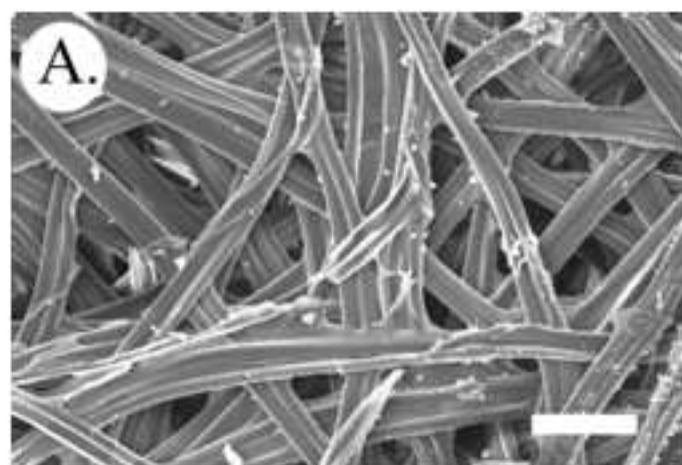
Fig. 7 (A) Basic FE model design and elements. (B) The load-displacement curves for *A. pernyi* model I (strong network and *A. pernyi* fibre properties extracted from Fig. 3B), intermediate model (weak network and *A. pernyi* fibre properties extracted from Fig. 3B) *B. mori* model I (weak network and *B. mori* fibre properties extracted from Fig. 3A). (C) The load-displacement curves for cocoon models with strong network and fibre properties extracted from reference [8]: *A. pernyi* model II; *B. mandarina* model; *B. mori* model II; *G. postica* model and *O. eucalypti* model, where  $F^* = \frac{F}{\sigma_{0,fibre} S_{fibre}}$  ( $F$  is the reaction force,  $\sigma_0$  is the yield stress of the fiber and  $S_{fiber}$  is the sectional area of the fiber) and  $d^* = \frac{d}{l}$  ( $d$  is the tensile displacement;  $l$  is the length of the network structure).



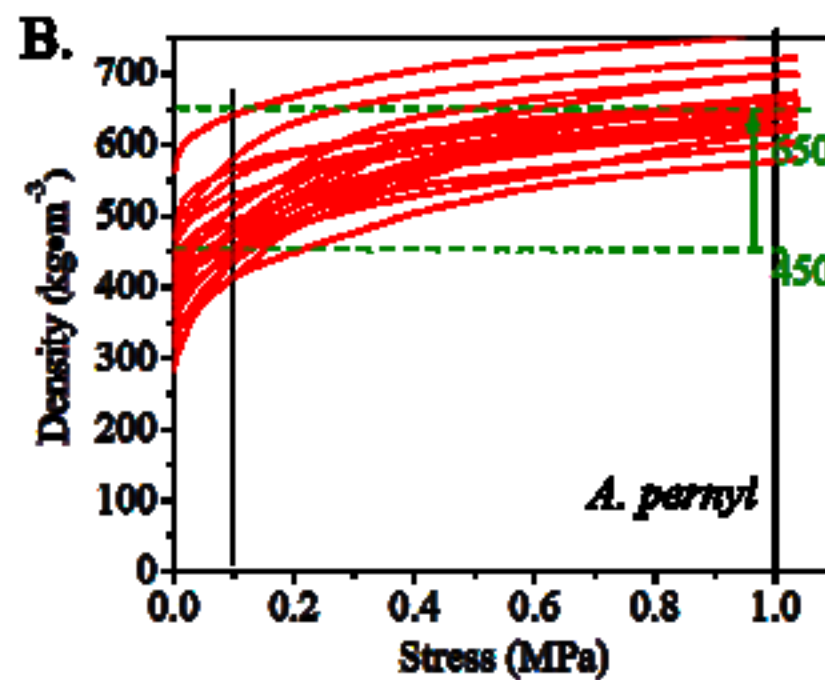
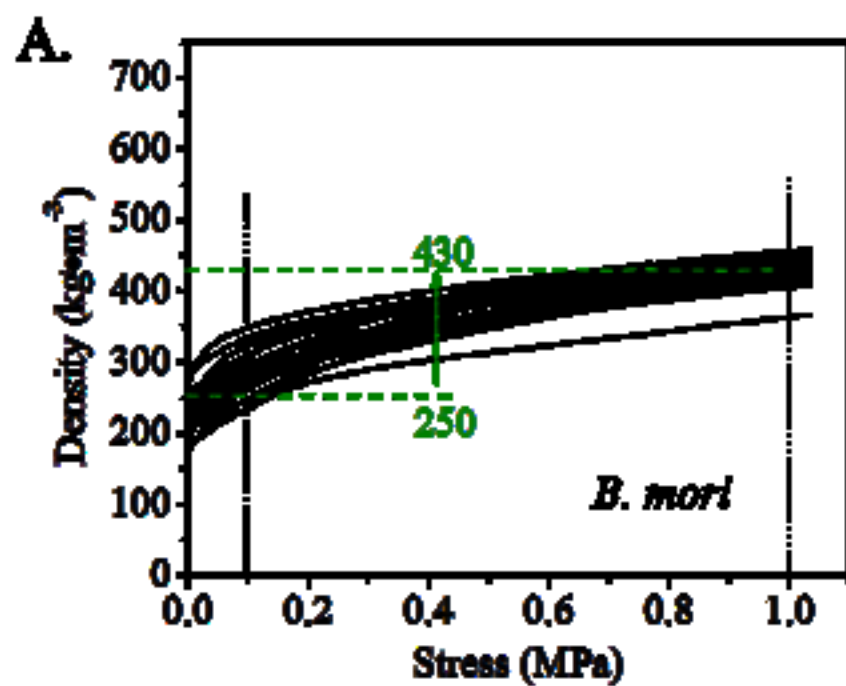


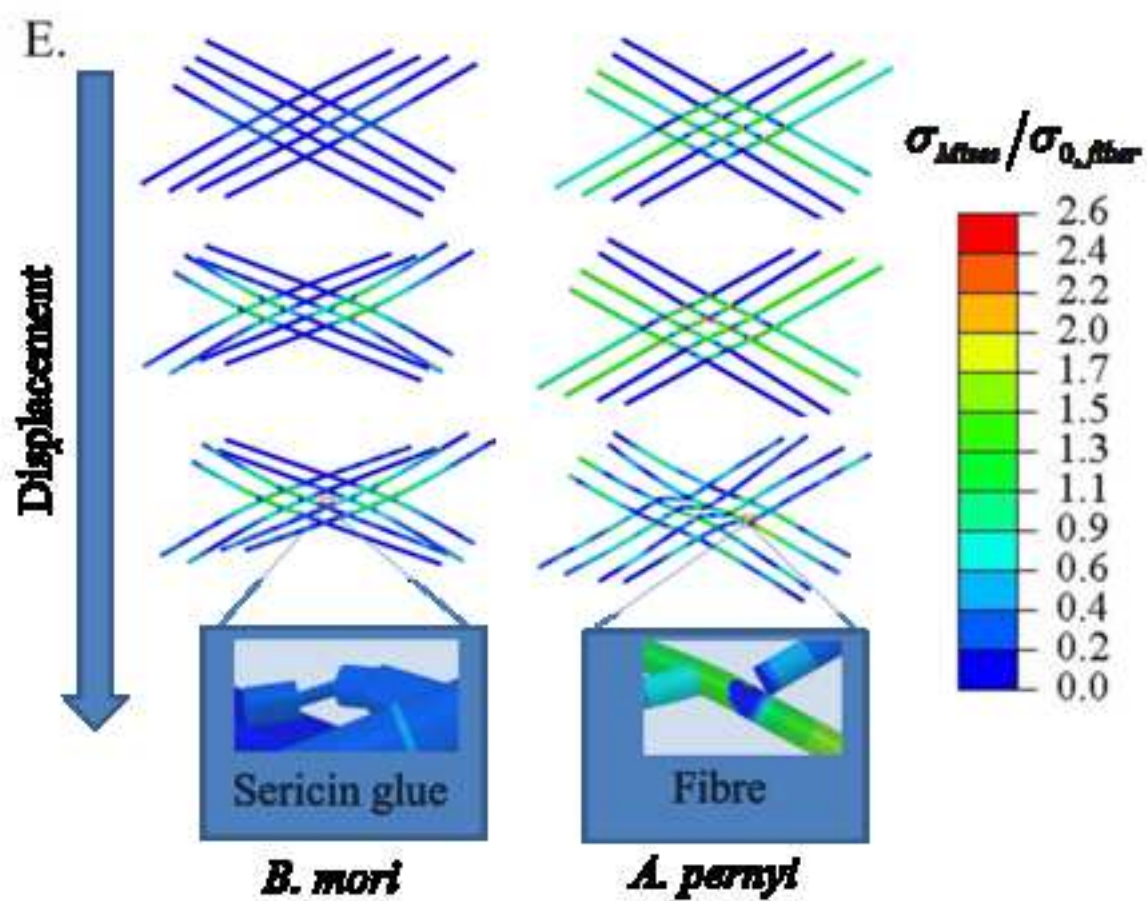
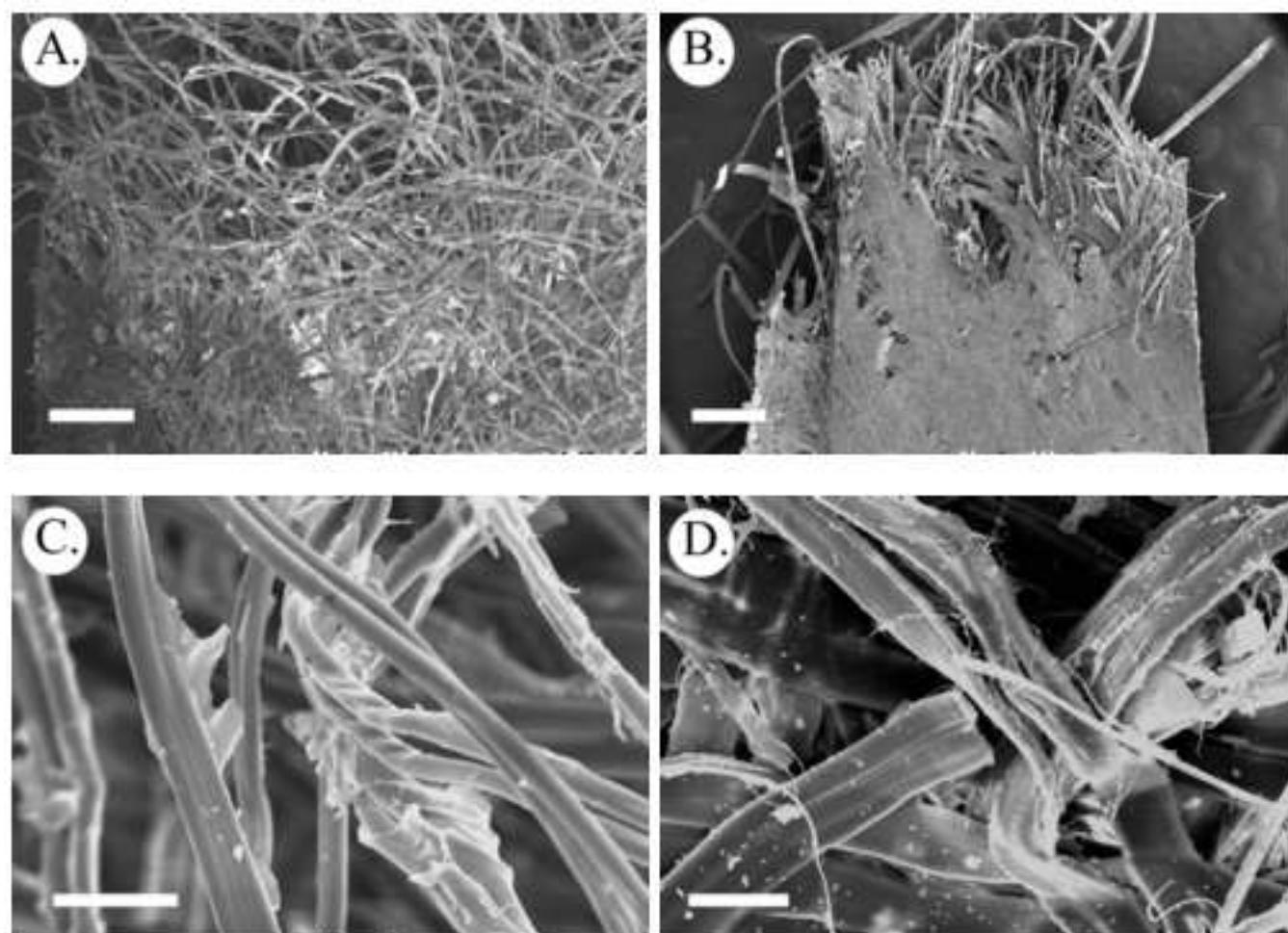


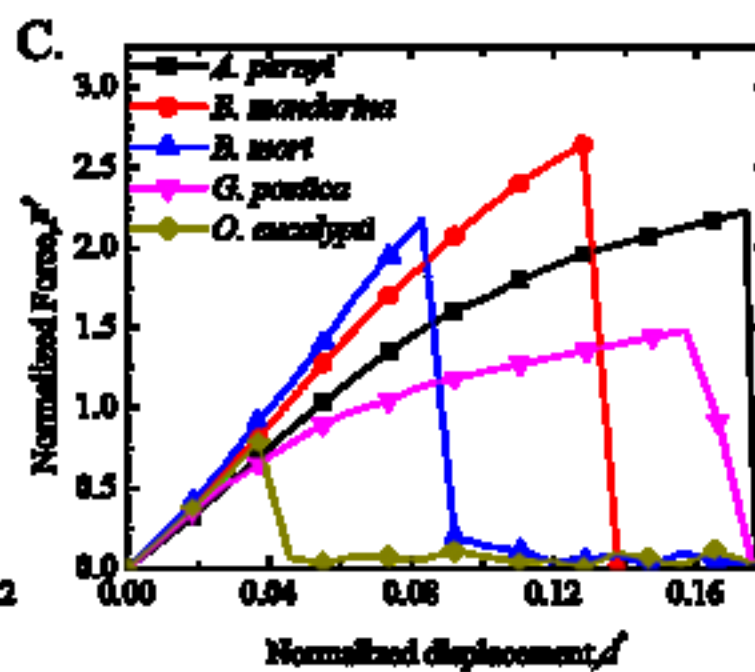
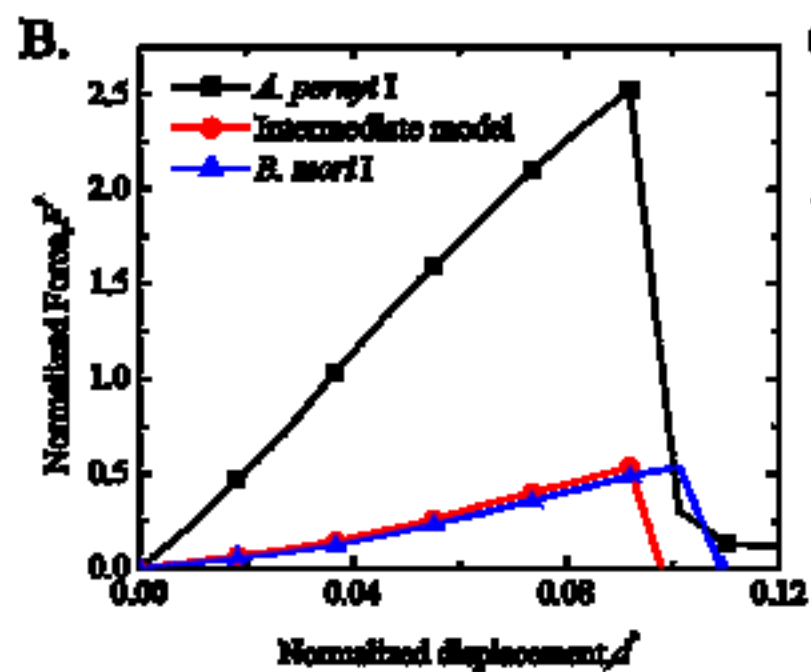
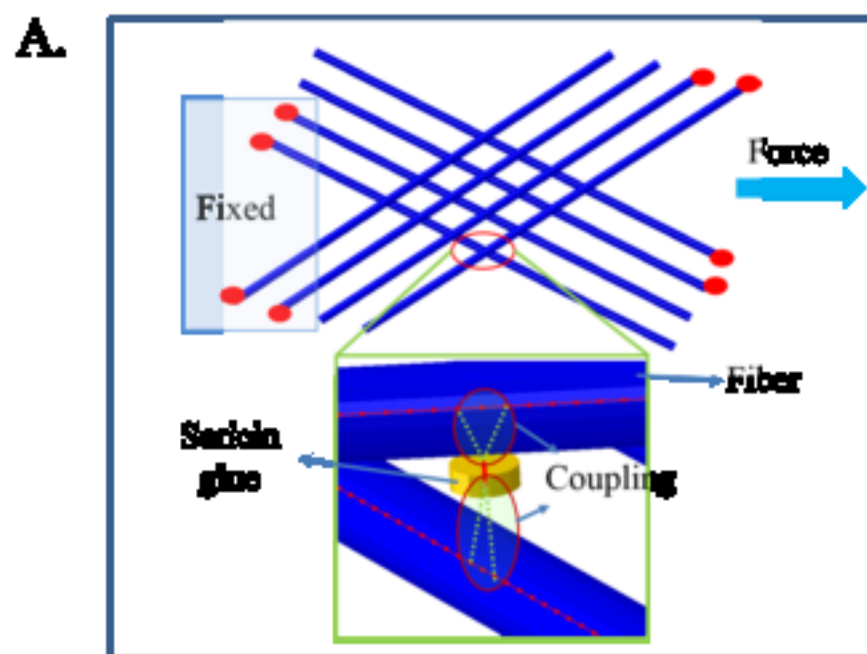


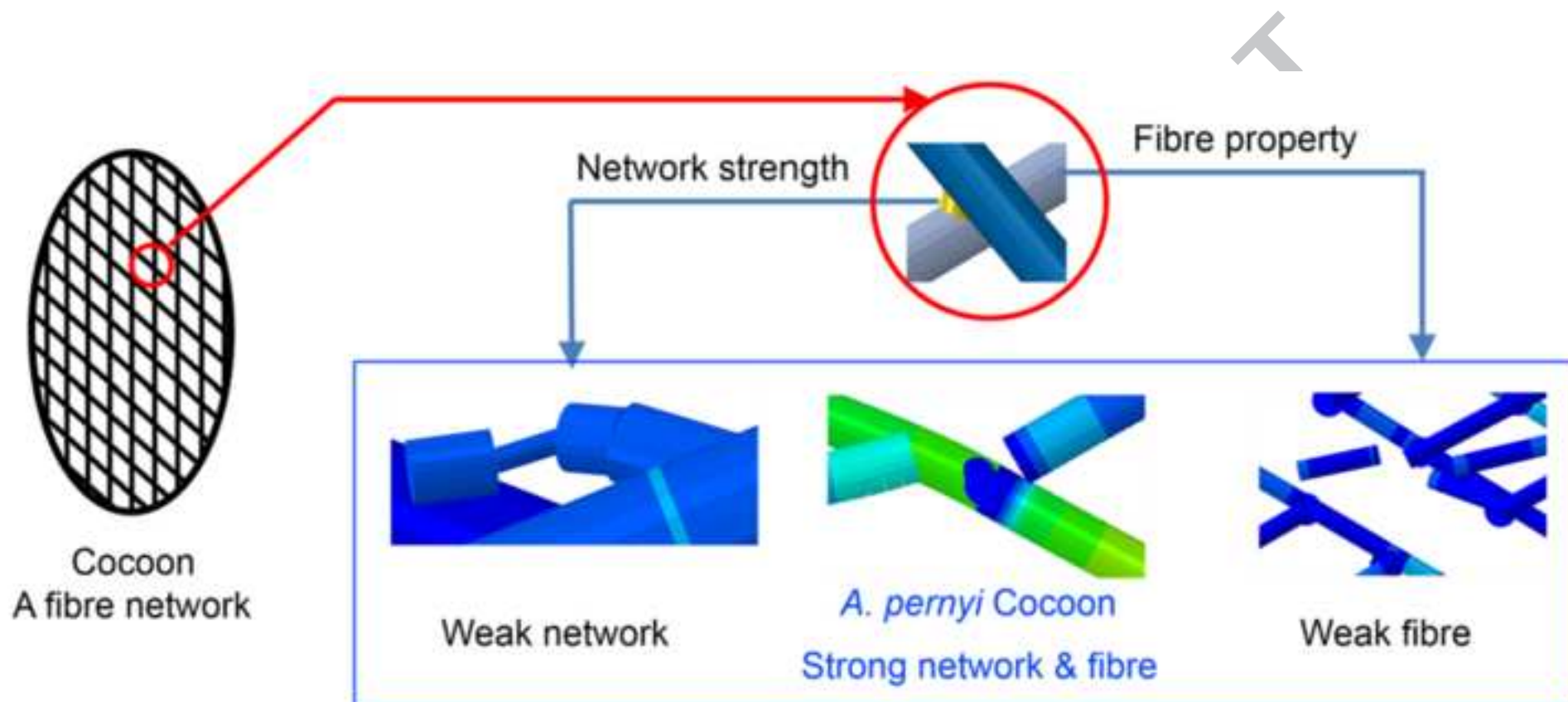












### Statement of Significance

Natural cocoons are an important group of natural fibre composites with versatile functionalities. Previous studies have focused on the diversity of cocoon species and the different morphological and mechanical features. It was suggested that the cocoon network structure determined the final mechanical properties of the cocoon composite. Nevertheless, the full structure-property-function relationships for the cocoon composite are not understood. Through studying two distinct cocoon species with specific functionalities, we prove that the mechanical properties of two cocoons are determined by both the network properties and the fibre properties. A robust fibre network is the prerequisite, within which the good mechanical properties of the fibres can play a part. The finding will inspire designs of synthetic composite with desirable and predictable mechanical properties.